BUTTERWORTH HEINEMANN

# Measurement in laminar and transitional boundary-layer flows on concave surface

D. H. Zhang, S. H. Winoto and Y. T. Chew
Department of Mechanical and Production Engineering, National University of Singapore, Singapore, Republic of Singapore

Measurements of streamwise mean and fluctuating velocities in laminar and transitional boundary-layer flows on a concave surface of 2.0 m radius of curvature have been performed using hot-wire anemometry technique. A new turbulent intermittency detector method was used to calculate the intermittency factor. In addition to the spanwise distributions of mean velocity, the profiles of mean, fluctuating velocities and intermittency across the boundary layer at two different spanwise positions; namely, the upwash and downwash, are also presented. The experimental results show that the normal and spanwise distributions of mean velocity, normal turbulence intensity $u'_{rms}/U_0$ profiles experience different streamwise evolutions in the laminar and transition regions. Significant velocity profile distortion, saturated growth of Goertler vortices, and the existence of two peaks in $u'_{rms}/U_0$ profiles are the main features of the boundary-layer flow at the onset of transition. The intermittency profiles in the early stages of transition at the two spanwise positions have some similar characteristics and are not consistent with each other on some other aspects. Comparisons of the $\gamma$ profiles at the two spanwise positions confirm that the transition first starts at the low-speed regions.

**Keywords:** boundary-layer flow; concave surface; laminar; transitional; measurement

## Introduction

It has been recognized that a strong inviscid instability may occur in laminar boundary-layer flows on concave surfaces with longitudinal curvature caused by the imbalance between centrifugal force and radial pressure gradient. This instability may result in steady counter-rotating streamwise vortices (now known as Goertler vortices). Since Goertler (1940) first predicted this phenomenon, numerous experimental and theoretical investigations have been made because of its effect in increasing heat transfer, (McCormack et al. 1970; Smith and Haj-Hariri 1993), and hastening boundary-layer transition from laminar to turbulence (Liepmann 1945). Goertler vortices can also be used in other fluid dynamic investigations that require counter-rotating vortices (Swearingen and Blackwelder 1987).

Based on the stability theory, for example, Goertler (1940), Smith (1955), and more recently Floryan and Saric (1982), Goertler vortices will develop in boundary layers over concave surfaces provided the Goertler number $G_\theta = U_0\theta/\nu(\theta/r)^{1/2}$, where $\theta$ is the Blasius boundary-layer momentum thickness exceeds a certain critical value. The presence of Goertler vortices makes the boundary-layer flow three-dimensional (3-D) because of the redistribution of the streamwise momentum, and therefore, causes spanwise variation in the streamwise velocity component and in boundary-layer thickness. That is, the boundary layer is thicker at upwash regions where the streamwise velocity is lower, and thinner at downwash regions where the velocity is higher.

Localized velocity measurements within the vortex system in laminar boundary layers have been made by using hot-wire anemometers; for example, Tani and Aihara (1969), Aihara and Sonoda (1981), Ito (1985), and Swearingen and Blackwelder (1987), and by using laser Doppler anemometer, for example, Winoto and Crane (1980). These works provide a large amount of information on the nonlinear evolution of Goertler vortices.

The problem of transition in the presence of Goertler vortices also attracts much attention. Tani and Aihara (1969) observed the vortex behavior near transition and concluded that Goertler vortices indirectly affect the transition by inducing a spanwise variation in the boundary-layer thickness. A secondary instability in the form of "horseshoe" vortices, as observed by Aihara and Sonoda (1981), Aihara and Koyama (1982), and Swearingen and Blackwelder (1987), seems to play a significant role in the onset of transition. Transverse oscillation of low frequency (known as vortex meandering), which seems to initiate the transition of the boundary layers was also found by Aihara (1979) and more recently by Swearingen and Blackwelder (1987).

The first boundary-layer transition experiment on concave surfaces was conducted by Liepmann (1945), who found that the presence of Goertler vortices can lower the transition Reynolds number. Recently, Crane et al. (1987) and Winoto and Low (1989) confirmed that the transition first started at the upwash regions by detecting the transition using a hot-film probe in a water channel and a hot-wire probe in a wind tunnel, respectively.

Address reprint requests to Dr. Winoto, Dept. of Mechanical and Production Engineering, National University of Singapore, 10 Kent Ridge Crescent, Singapore 0511, Republic of Singapore.

Received 1 August 1994; accepted 15 November 1994

Int. J. Heat and Fluid Flow 16: 88–98, 1995

655 Avenue of the Americas, New York, NY 10010

SSDI 0142-727X/95/$10.00
SSDI 0142-727X(94)00017-7

Many experimental studies on the evolution of Goertler vortices and their effect on the onset of transition have been reported. However, only relatively few systematic measurements in concave surface laminar and transitional boundary-layer flows have been performed, especially those that concentrate on the intermittency behavior. The aim of the present work is to provide more detailed information on the effect of Goertler vortices on the flowfield within the laminar and transitional regimes. Measurements of streamwise mean and fluctuating velocities and intermittency factor were carried out using the hot-wire anemometer technique.

## Experimental details

### Apparatus and instrumentation

The experiments were carried out in a perspex curved duct of rectangular cross-section, connected to a low-speed, blow-down-type wind tunnel. The duct is a 60° bend with cross-sectional dimensions of 0.15 m × 0.60 m. The perspex concave test surface, which has a constant radius of curvature of 2.0 m and a sharp leading edge with an acute angle of 15°, is mounted inside the duct at 0.05 m from the duct outer surface, forming a working test section with aspect ratio of six.

Flow is generated by a 0.60 m centrifugal fan powered by a 4.3 kW variable speed dc shunt-wound motor. The motor speed was thyristor controlled and adjusted manually, giving stability of flow velocity in the wind tunnel better than 1 percent throughout its speed range. A small angle (11 1/4°) diffuser connects the blower to a 0.60 m × 0.60 m settling chamber. To prevent the transmission of vibration caused by the fan, a 5 mm-thick rubber pad was installed between the fan section and the diffuser.

The upstream portion of the settling chamber consists of a honeycomb with cells of 10 mm diameter and 50 mm length, and five removable frames, each having interior dimensions of 0.61 m × 0.61 m × 0.02 m. Fine screens of mesh 20 (per inch) and 28 s.w.g (0.38 mm diameter) stainless steel wire gauze are attached to the frames. A two-dimensional (2-D) 4:1 contraction is attached downstream to the settling chamber, which reduces the flow cross-sectional area to that of the rectangular curved duct.

A single sensor hot-wire probe having a platinum-plated tungsten wire of 1.25 mm long and 5 $\mu$m diameter, operated by a constant temperature anemometer (CTA) system at an overheat of 1.5, was used to obtain the streamwise velocity component and free-stream turbulence intensity data. This probe is mounted on a traversing mechanism that is placed on the top surface of the test section and is capable of traversing in the streamwise $x$, normal to the surface $y$ and spanwise $z$ directions. The access of the probe to the concave surface is achieved by inserting it through a large opening made on the top surface. This opening is covered by a thin, well-fitted perspex plate that can slide on the top surface of the test section. The streamwise distance $x$ from the leading edge and the spanwise position $z$ were measured by means of fine ink marks on the test surface. The estimated errors are within 1 mm. A traveling microscope that gave a reading accuracy of $\pm$0.01 mm was used to determine the distance between the test surface and the probe. The zero-position of the probe was determined by using "mirror method" with an accuracy of about 0.05 mm.

The voltage signal from the CTA was first low-pass filtered to reduce any high-frequency noise associated with the electronic circuitry, and then simultaneously fed into a digital voltmeter, an rms-unit, and a signal conditioner. The voltmeter and the rms-unit were, respectively, used to obtain local mean and rms-fluctuating velocities (an average time of 30 seconds was used). The signal conditioner was used to condition signals for calculating turbulent intermittency. To eliminate the effect of the large-scale unsteadiness on the calculation of intermittency factors, a 200 Hz high-pass filter was used to remove any mean and low-frequency components of signals before being digitized with a 12-bit A/D converter at a sampling frequency of 2 kHz. The duration for each sample was taken to be 20.48 seconds, which was considered adequate to produce a statistically stationary results. Further increase in the duration of sampling time results in the scatter of intermittency values obtained at a fixed point to be less than 2 percent for the same flow condition. The data obtained were stored in a microcomputer memory. In addition, a dual-beam oscilloscope was also used to monitor the signals simultaneously.

### Detection of turbulent intermittency

In this work, a new intermittency detection method was used to determine the turbulent intermittency factors (Zhang et al. 1994). In this method, the quantities of $\overline{|u' \partial u'/\partial t|}$ over a predefined time-interval (0.005 seconds, which equals the

## Notation

| | |
|---|---|
| $C$ | dimensional constant for threshold |
| $C_p$ | static pressure coefficient $(P - P_R)/1/2\ \rho U_R^2$ |
| $G_\theta$ | Goertler number $U_0\ \theta/\nu\ (\theta/r)^{1/2}$ |
| $H$ | shape factor $\delta^*/\theta$ |
| $p$ | static pressure |
| $P_R$ | reference static pressure measured at $x$ = 200 mm |
| $\mathrm{Re}_x$ | Reynolds number based on streamwise distance $U_0 x/\nu$ |
| $U_0$ | free-stream velocity |
| $U_R$ | reference free-stream velocity at $x$ = 200 mm |
| $r$ | radius of concave surface |
| $t$ | time |
| $\bar{u}$ | streamwise mean velocity |
| $u'$ | streamwise fluctuating velocity |
| $u'_{\mathrm{rms}}$ | root-mean-square value of streamwise fluctuating velocity |
| $(u'_{\mathrm{rms}})_{\max}$ | maximum value of $u'_{\mathrm{rms}}$ across boundary layer |
| $x$ | coordinate in streamwise direction (measured from concave surface leading edge) |
| $x_{\mathrm{tr,s}}$ | transition start position |
| $x_{\mathrm{tr,e}}$ | transition end position |
| $y$ | coordinate normal to concave surface (measured from concave surface) |
| $z$ | coordinate in span-wise direction (measured from centerline of concave surface) |

*Greek*

| | |
|---|---|
| $\gamma$ | turbulent intermittency factor |
| $\delta^*$ | boundary-layer displacement thickness |
| $\theta$ | boundary-layer momentum thickness |
| $\eta$ | nondimensional parameter $y/(x\nu/U_0)^{1/2}$ |
| $\nu$ | fluid kinematic viscosity |
| $\xi$ | nondimensional parameter $(x - x_{\mathrm{tr,s}})/(x_{\mathrm{tr,e}} - x_{\mathrm{tr,s}})$ |
| $\rho$ | fluid density |

reciprocal of the lowest frequency of the flow signals after the high-pass filter) and $C(\bar{u}(\partial u'/\partial t)_{rms}/(u'\partial u'/\partial t)_{rms})$ were respectively used as the turbulent detector function and the corresponding threshold level. When $\overline{|u'\,\partial u'/\partial t|} \geq C(\bar{u}(\partial u'/\partial t)_{rms}/(u'\,\partial u'/\partial t)_{rms})$, the corresponding flow in the predefined time-interval was regarded as turbulent, otherwise as laminar. Each flow record consists of a number of time intervals, the intermittency value of the record is determined by the ratio of the number of turbulent time intervals to the total number of time intervals in the record. In the above equation, $u'$ and $\bar{u}$ are the streamwise fluctuating and local mean velocities; $C$ is a threshold constant and was taken to be two according to the experiments; $(\partial u'/\partial t)_{rms}$ and $(u'\partial u'/\partial t)_{rms}$ are both the long time standard deviations.

By testing this method in transitional boundary-layer flows (Zhang et al. 1994), it was found that it had several advantages, such as: (1) its nonlinear detector function $u'\,\partial u'/\partial t$ can widen the range of values of a transitional flow signal caused by nonlinear amplification that results in clearer discrimination between laminar and turbulent patches; (2) its threshold value is more stable and less sensitive to the choice of value of the constant $C$ when compared with other methods; and (3) it gives more reliable intermittency values in the near wall region of a transitional boundary layer (see also Kuan and Wang 1990).

### Flow conditions and experimental procedure

Before the experiments, measurements of free-stream velocity outside the boundary layers in the test section showed that the spanwise deviation was within 1 percent for the free-stream velocity range from 4.0 to 15.0 m/s. In this range, the free-stream turbulence intensity at various streamwise positions was about 0.3 percent.

The measurements reported here were conducted for free-stream velocity $U_0 = 6$ m/s, in which the streamwise static pressure distribution (obtained from the static pressure taps installed along the midspan of the test surface and connected to a digital manometer with an accuracy of 0.01 mm $H_2O$), showed deviation of static pressure coefficient $C_p = 2(p - p_R)/\rho U_R^2$ to be less than 2 percent, where $p_R$ and $U_R$ are, respectively, the reference static pressure and free-stream velocity measured at $x = 200$ mm. In the experiment conducted by Swearingen and Blackwelder (1987), the deviation of $C_p$ was 1 percent.

The hot wire was calibrated in the free-stream region (over the range of velocities to be encountered within the boundary layer) against a standard Pitot tube that was connected to a micromanometer with a reading accuracy of 0.008 mm $H_2O$. The mean voltages obtained by the microcomputer from the CTA outputs, together with the readings from the micromanometer were used to obtain the least-squares estimates of the constants $A$ and $B$ in the relation $E^2 = A + BU^{0.45}$, where $E$ is the anemometer voltage, and $U$ is the mean velocity. Prior to the static calibration, the frequency response of the constant temperature hot-wire anemometer was adjusted at the maximum velocity expected in the subsequent experiment. Applying the square-wave test, a frequency response typically greater than 10 kHz was achieved for the 5 $\mu$m diameter sensor connected to a 5-meter probe cable. Calibration of the hot-wire was carried out before each set of measurements. During each set of measurements, the calibration was checked frequently against the free stream, which was monitored constantly by a Pitot probe. When there was a drift of more than 2 percent, the corresponding data will be rejected and, the calibration and the measurements will be repeated. By adopting the above measures, it was estimated that the velocity can be measured to an accuracy of about 1 percent.

For extensive investigation of the flowfield, the quantities of

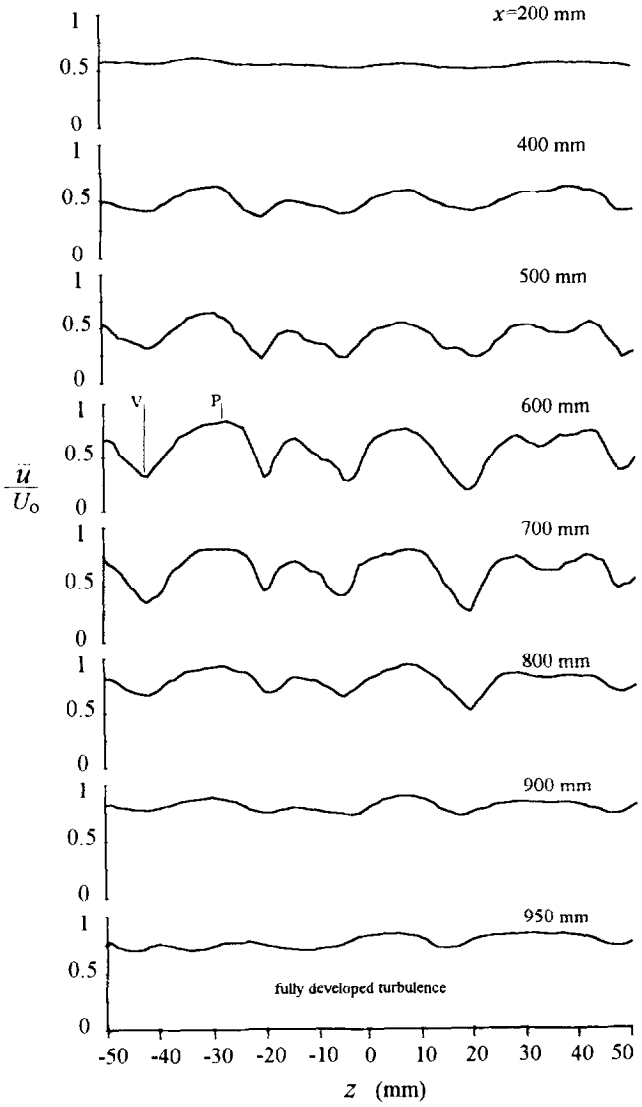


*Figure 1* Mean streamwise velocity distributions in the spanwise direction at fixed $y/\theta = 2$ and various streamwise positions. *P* and *V* correspond to a downwash and an upwash region, respectively

$\bar{u}(z)$, $\bar{u}(y)$, and $u'_{rms}(y)$ were measured within the boundary layer for a number of streamwise locations covering the laminar and transitional regions, from $x = 200$ mm ($G_\theta = 2.86$, and $Re_x = 0.78 \times 10^5$) to $x = 950$ mm ($G_\theta = 9.17$, and $Re_x = 3.73 \times 10^5$). Measurements of the mean streamwise velocity component was first carried out in the spanwise direction at a fixed distance of $2\theta$ from the test surface (where $\theta$ is the boundary-layer momentum thickness calculated using the Blasius flat-plate solution). This was done to find the peaks and valleys in the resulting spanwise distributions $\bar{u}(z)$ that correspond to downwash and upwash regions, respectively, and hence, indicate the presence of streamwise counter-rotating Goertler vortices (Figure 1). Spanwise positions *P* (downwash region) and *V* (upwash region) were then chosen (Figure 1) for the measurements of $\bar{u}(y)$ and $u'_{rms}(y)$ at various streamwise locations.

## Results and discussion

### Mean flowfield

The spanwise velocity $\bar{u}(z)$ distributions, at eight streamwise locations (Figure 1) show the development of the flowfield in

the streamwise direction and the presence of the Goertler vortices in the boundary-layer flow. The $\bar{u}(z)$ distributions seem to experience two stages in their streamwise development:

(1) In the laminar region (for $x \leq 600$ mm, $G_\theta \leq 6.53$), the initial boundary layer seems to be unperturbed in the spanwise direction in the early stage (for $x \leq 200$ mm), but from $x = 400$ mm onward, the effect of Goertler vortices becomes evident. The boundary layer becomes 3-D because of alternate regions of high- and low-speed fluid in the spanwise direction, and hence, causing the spanwise profiles $\bar{u}(z)$ to be inflexional. With

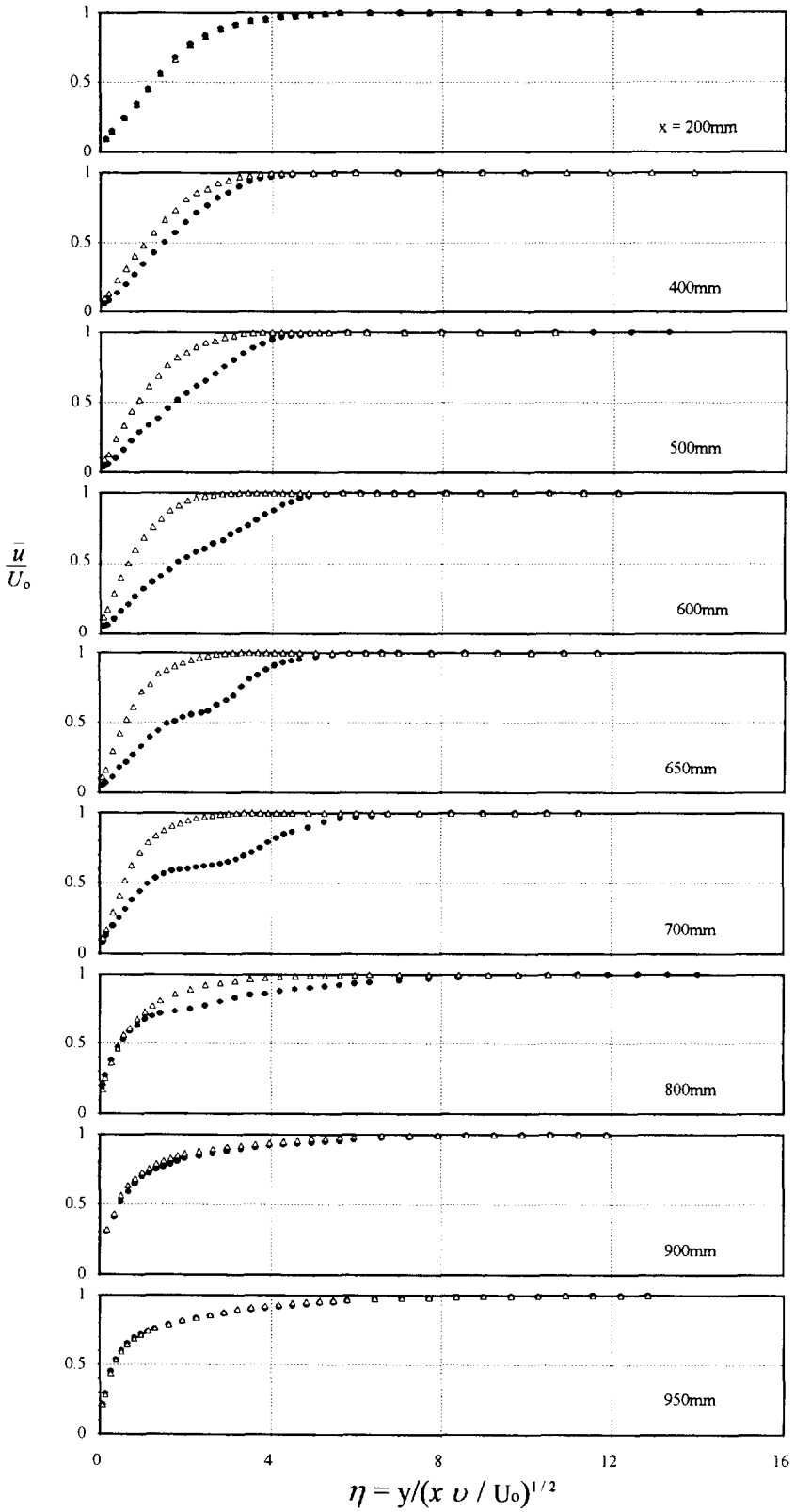


*Figure 2* Profiles of mean streamwise velocity at various streamwise positions. (• = upwash region *V*; △ = downwash region *P*)

increasing streamwise distance, each of the high-speed (downwash) and low-speed (upwash) regions maintains the fixed spanwise positions, but the difference between the velocities in the upwash and downwash regions gradually becomes larger, and eventually reaches a saturation at $x = 600$–$700$ mm. Meanwhile, as the vortex flow evolves, the high-speed region becomes wide and flat, and the low-speed region becomes narrow and sharp. These are in complete agreement with the results of Swearingen and Blackwelder (1987), Winoto and Crane (1980), Ito (1985), and Winoto and Low (1989).

(2) In the transition region (for 640 mm $\leq x \leq$ 950 mm), the additional mixing caused by the occurrence of transition smears out the laminar spanwise structure and exerts significant influences on the flowfield. This makes the spanwise distributions homogeneous downstream. At the same time, the upwash and downwash regions are not at the same spanwise positions when the fully turbulent flow is reached ($x = 950$ mm).

Profiles of $\bar{u}/U_0$ against a nondimensional boundary-layer parameter $\eta(=y/xv/U_0)^{1/2})$ at the eight downstream locations are shown in Figure 2 for spanwise positions $V$ (upwash region) and $P$ (downwash region). These profiles are similar to those of Ito (1985) and Swearingen and Blackwelder (1987). In the upstream region (for $x \leq 200$ mm), the mean flow develops almost in the same way as Blasius boundary layer. The experimental data obtained at the upwash and downwash regions agree very well with each other, and the velocity distributions are all of Blasius type. At $x = 400$ mm, the difference of velocity in the upwash and downwash regions becomes apparent as the Goertler vortices evolve progressively. The profiles show a defect from the Blasius flow in the upwash region and an increase in the downwash region, which becomes more apparent with increasing streamwise distance. Distortions from the Blasius flow gives rise to concentrated regions of low- and high-speed fluid that produce a boundary layer with wavy appearance in the spanwise direction as its thickness alternately increases and decreases. Consequently, the velocity distribution $\bar{u}(z)$ becomes inflexional across one spanwise wavelength. Up to $x = 600$ mm, the velocity profile $\bar{u}(y)$ obtained in the upwash region also begins to become inflexional, and this situation is more apparent at $x = 650$ and 700 mm. These inflexional profiles appear in the same region where the amplitude growth of the spanwise distribution reaches a saturation. In addition, the boundary-layer flow also becomes transitional here (from turbulent intermittency measurements, $\gamma$ starts to become nonzero at $x = 640$ mm). In the transition region (for $x = 640$–$950$ mm), as the boundary-layer flow becomes more turbulent, the additional mixing gradually reduces the difference between the velocity distributions at the upwash and downwash regions. At $x = 950$ mm, both the upwash and downwash distributions become turbulent type, and the difference between them is diminishing.

The streamwise developments of the measured displacement thickness $\delta^*$, momentum thickness $\theta$, shape factor $H$, and Goertler number $G_\theta$ in the laminar and transitional regions at the upwash and downwash positions are compared with the corresponding Blasius growths (Figure 3). At upwash, $\delta^*$ begins to increase at about $x = 350$ mm and continues until reaching a maximum near $x = 650$ mm, where the growth of the streamwise vortices reaches saturation and, at the same time, the transition starts. At downwash, $\delta^*$ decreases at $x = 500$ mm, and reaches a minimum at about $x = 650$ mm, where its value is about half of that of the upwash. After the flow becomes transitional, because of the existence of additional mixing, $\delta^*$ begins to decrease and increase, respectively, in the upwash and downwash regions, and eventually reaches a similar value at $x = 950$ mm, where the boundary-layer flow becomes fully turbulent. The measured $\delta^*$ is lower than its Blasius laminar value at $x = 950$ mm.

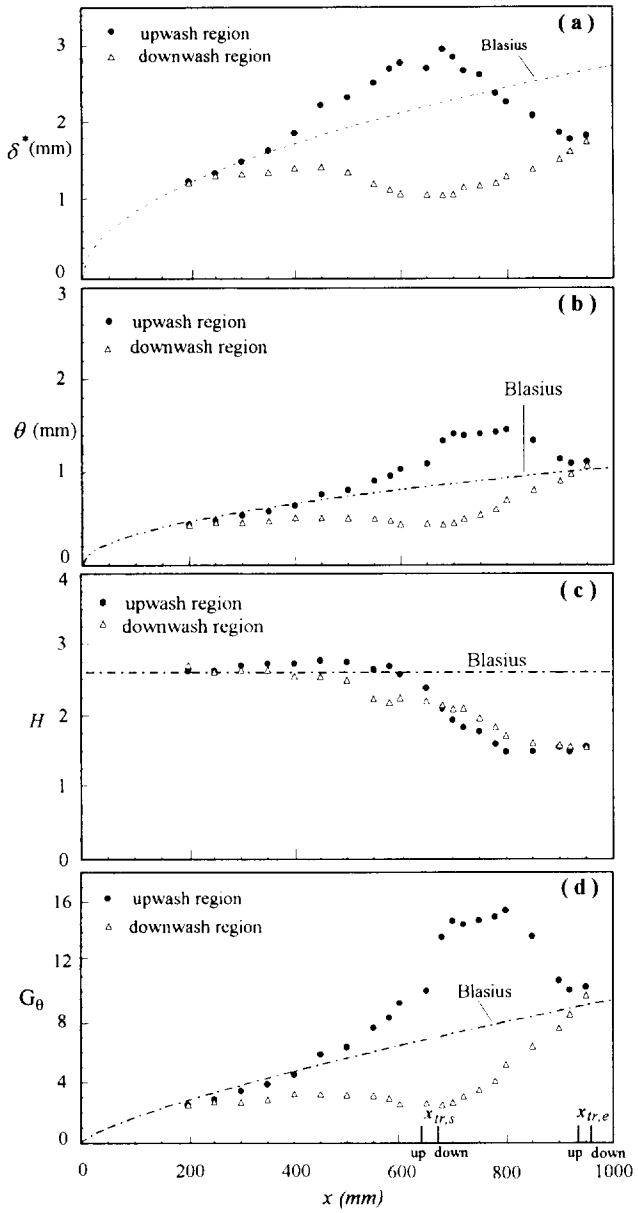


*Figure 3* Streamwise development of the boundary-layer parameters in the upwash and downwash regions. (a) = displacement thickness; (b) = momentum thickness; (c) = shape factor; (d) = Goertler number

For the streamwise development of the measured $\theta$, a similar situation exists at both upwash and downwash. Compared with that for $\delta^*$, $\theta$ in the upwash region begins to grow at 450 mm and reaches its peak at 750 mm. At downwash, $\theta$ varies in a similar manner as $\delta^*$ at some stages.

As shown in Figure 3c, the development of the shape factor $H$ from laminar to turbulent flow, both in the upwash and downwash regions, is similar to the case of a flat-plate boundary-layer flow. The variation of $H$ with $x$ in the downwash region is less distinct than that in the upwash region.

Because the Goertler number $G_\theta$ is obtained based on the momentum thickness $\theta$, its streamwise developments at the upwash and downwash regions are quite similar to the case of

$\theta$, and shown in Figure 3b and d. However, based on the measured values of $\theta$, $G_\theta$ in the transition start-region (for $x = 650$–$700$ mm) are much higher in the upwash region and much lower in the downwash region than those based on Blasius values. This suggests that when a transition Goertler number criterion is used, the difference between the upwash and downwash regions should be taken into account. The criterion based on the Blasius value can roughly reflect the average situation in relation to the upwash and downwash regions. It is interesting to note that, at $x = 650$ mm, which represents the approximate transition start position (transition begins at 640 mm and 675 mm for upwash and downwash regions, respectively). Their average value of 6.33 agrees well with the empirical transition Goertler number criterion of $G_\theta = 6$ suggested by Liepmann (1945) on a concave surface with a constant radius of curvature of 2.5 ft at free-stream turbulence of 0.3 percent without considering the spanwise boundary-layer variation.

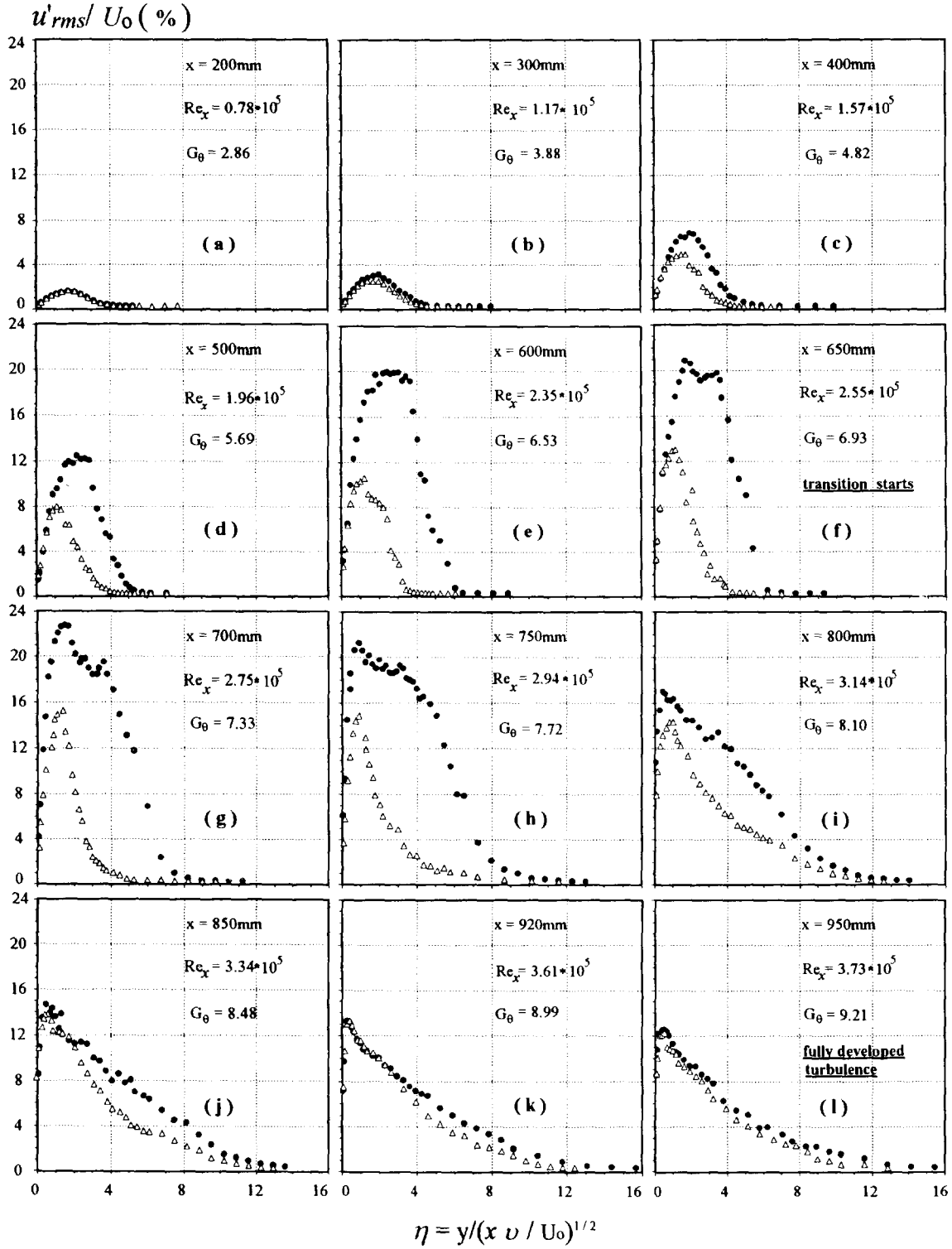


*Figure 4* Profiles of $u'_{rms}/U_0$ at various streamwise positions. (• = upwash region $V$; △ = downwash region $P$)

### Streamwise turbulence intensity

The streamwise root-mean-square velocity fluctuations, $u'_{rms}$, within the two spanwise regions of the boundary layer were measured at the same time as the mean velocity. The normal profiles of $u'_{rms}$ normalized by $U_0$ (streamwise component of turbulence intensities) at various streamwise locations are also plotted against the parameter $\eta (= y/(xv/U_0)^{1/2})$, as presented in Figure 4. This figure shows that, in the measurement range from $x = 200$ mm ($Re_x = 0.78 \times 10^5$) to $x = 950$ mm ($Re_x = 3.73 \times 10^5$), the relation between the $u'_{rms}/U_0$ profiles at the upwash and downwash regions for each streamwise location is similar to that of the mean velocity during the evolution with $x$. In the early stage (for $x \leq 200$ mm), the effect of Goertler instability on the boundary-layer flow is weak, so the profiles at the two spanwise positions coincide. (The existence of turbulence-like profiles in the laminar region is believed caused by three-dimensionality of the boundary layers). At $x = 300$ mm, with the occurrence of the inflexional distribution of $\bar{u}(z)$, the maxima of $u'_{rms}/U_0$ profiles increase both at the upwash and downwash, and the difference between them also begins to appear. As reported by Swearingen and Blackwelder (1987), in the upwash vicinity, the shear of $\partial\bar{u}/\partial z$ is high, which makes the $u'_{rms}/U_0$ increase more rapidly in the upwash region than in the downwash region. As this kind of spanwise shear (at upwash) and the streamwise shear in $\bar{u}(y)$ (at downwash) become stronger downstream, the maxima of $u'_{rms}/U_0$ profiles at both upwash and downwash and their difference become larger. This situation continues to $x$ about 650–700 mm, where the inflexional-type profile distortion in $\bar{u}(z)$ saturates, and the $\bar{u}(y)$-profile in the upwash region also becomes inflexional. The maxima of the $u'_{rms}/U_0$ profiles at the two spanwise positions reach their highest values, and their maximum difference also occurs. At the same time, the flow becomes transitional. In the following stage, starting at $x = 750$ mm, because of the breakdown of Goertler vortices, the spanwise and streamwise shears caused by the vortices decrease gradually. This results in a decreasing $u'_{rms}/U_0$ both in the upwash and downwash regions, with the value in the upwash region decreasing more quickly. Up to $x = 950$ mm, where the boundary-layer flow becomes fully turbulent, the $u'_{rms}/U_0$ profiles at the two different spanwise regions again coincide.

By examining the upwash and downwash $u'_{rms}/U_0$ profiles at various streamwise locations, some characteristic features can be identified. The upwash profiles at positions $x = 200$ mm–600 mm exhibit round peaks at around $\eta = 2$, as their maximum values become larger with increasing $x$, as shown in Figure 4a–e. At $x = 650$ mm when transition begins, two sharp peaks appear in the $u'_{rms}/U_0$ profile at upwash, as shown in Figure 4f. It is interesting to note that the normal positions of the first peak at $x = 650$ mm and 700 mm are near the first inflexional points in the corresponding normal mean velocity profiles (Figure 2), and the positions of the second peaks correspond to those of the second inflexional points in the $\bar{u}(y)$-profiles. This suggests that, in addition to the high shear in $\partial\bar{u}/\partial z$, which results in high values of $u'_{rms}/U_0$, as pointed out by Swearingen and Blackwelder (1987), the high $\partial\bar{u}/\partial y$ might also exert some influences in producing high fluctuations. This is in accordance with the findings of Swearingen and Blackwelder that there are regions of strong $\partial\bar{u}/\partial y$ shear near the positions of inflexion in the $\bar{u}(y)$-profiles. The existence of the second peak in $u'_{rms}/U_0$ profiles may be caused by the occurrence of some secondary instabilities in the region. According to some previous work (see Floryan 1991; Saric 1994), the breakdown process of Goertler vortices is through a secondary instability that occurs when the vortex motion begins to saturate while distorting the mean flow. Aihara and Koyama (1982) and Ito (1985) observed a periodic formation of horseshoe-type vortices on both sides of the upwash region in the outer boundary layers through flow visualizations. In the present work, the existence of such vortices formed at the high shear layers above the second inflexional point (i.e., near the edge of the boundary layer) around the upwash region might lead to the occurrence of the second peak in $u'_{rms}/U_0$ profiles, and then to transition to turbulence through their chaotic breakdown.

At the downwash, the $u'_{rms}/U_0$ profiles at $x = 200$, 300, and 400 mm share the same features as those at the upwash, but their maxima are of lower magnitudes. However, in the region $x = 400$ mm–700 mm, the peaks at downwash are closer to the wall (around $\eta = 1$), as compared with the case for the upwash. This might be attributable to thinner boundary layer at the downwash. Again, no obvious second peaks of $u'_{rms}/U_0$ profiles were observed at the downwash. But, as for the streamwise evolution of $u'_{rms}/U_0$ within the transition region, some similarities exist with respect to the upwash and downwash. The highest peak value of $u'_{rms}/U_0$ profiles at the downwash also appears at $x = 700$ mm. After reaching its highest value, it decreases with $x$ to the value of the turbulent boundary-layer flow.

The streamwise evolutions of $u'_{rms}/U_0$ are represented by the streamwise variations of the maxima of $u'_{rms}/U_0$ profiles for the upwash and downwash (Figure 5). Their trends in the laminar and transitional regions are similar to the results of Kuan and Wang (1990) for the flat-plate boundary layer. The highest value at the downwash (about 0.16) agrees very well with the those of Klebanoff et al. (1962), and Kuan and Wang (1990) for flat-plate transitional boundary-layer flows. The much higher value of $u'_{rms}/U_0$ at the upwash in the present study might be caused by the existence of higher shear in this region, caused by the presence of Goertler vortices. In addition, it is observed that the maxima of $u'_{rms}/U_0$ at both spanwise positions grow slowly in the laminar and early transitional regions. After they reach their maximum values, they begin to decrease rapidly to an equilibrium value of about 0.12 in the fully turbulent flow. This might indicate the possible existence

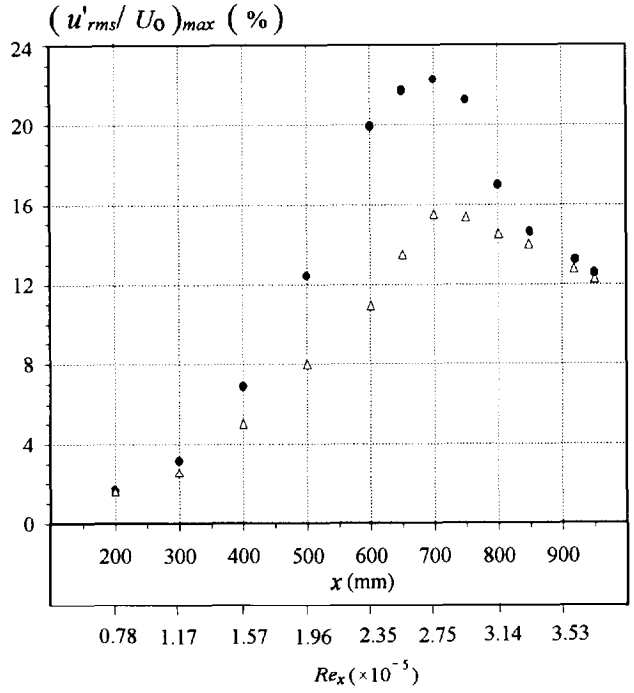


*Figure 5* Evolution of maximum of $u'_{rms}/U_0$ in the streamwise direction. (● = upwash region $V$; △ = downwash region $P$)

of secondary instability in the form of horseshoe-type structures caused by the interactions of Goertler vortices with the spanwise vorticities attributable to Kelvin–Helmholtz instability (Floryan 1991), which results in the rapid collapse of Goertler vortices during transition.

### Intermittency factor

The profiles of the intermittency factor $\gamma$ across the boundary layer obtained at the upwash and downwash regions for various streamwise locations are presented in Figures 6 and 7. The streamwise location is presented by a nondimensional parameter $\xi = (x - x_{tr,s})/(x_{tr,e} - x_{tr,s})$, where $x_{tr,s}$ and $x_{tr,e}$ are, respectively, the transition start and end positions determined by $\gamma$ whose maximum value across the boundary layer first becomes nonzero at $x_{tr,s}$, and first reaches a unity at $x_{tr,e}$.

As shown in Figures 6 and 7, the intermittency profiles for the upwash and downwash regions in the early stages of transition exhibit the same behavior that the $\gamma$ does not decreases monotonically with increasing $y$ from the wall to the outer flow. Instead, a fairly constant maximum value midway across the boundary layer in the upwash region, and a peak near the wall ($\eta \approx 1$) in the downwash region are, respectively, observed at $\gamma < 0.9$. This suggests that, in the early stages of transition, the most vigorous turbulent activity takes place midway across the boundary layers at the upwash transitional region, and occurs at $\eta \approx 1$ at the downwash.

An interesting point to note is that the maximum $\gamma$ at $x = 650$ mm in the upwash region occurs at $\eta \approx 3$–4, which corresponds to the positions of the high shear region above the second inflexional point (i.e., near the edge of the boundary layer) in the corresponding $\bar{u}(y)$ profile, and of the second peak in the $u'_{rms}/U_0$ profile. This, to a certain extent, indicates that the transition might start in this region because of the breakdown of the streamwise vortices under the influence of some other secondary instabilities, as mentioned previously. Downstream of $x = 650$ mm, the transitional boundary layer at the upwash may be influenced by the further breakdown of Goertler vortices and the turbulent spots generated near the wall, resulting in a fairly constant $\gamma$ midway across the boundary layer.

Because the downwash boundary layer resembles that on flat plates, the characteristics of the transition in this region should

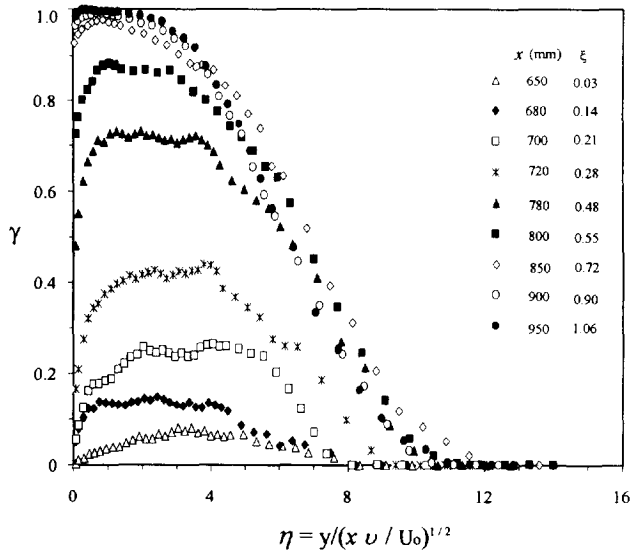


*Figure 6* Distributions of intermittency across the boundary layer at various streamwise positions in the upwash region *V*

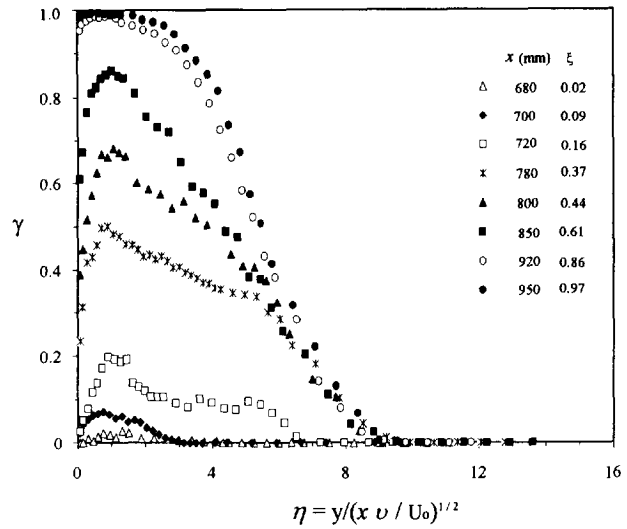


*Figure 7* Distributions of intermittency across the boundary layer at various streamwise positions in the downwash region *P*

have strong similarities to that on flat plates. By comparing the present results with those of Kuan and Wang (1990) and Sohn et al. (1991) for the flat-plate boundary layers, it is found that the $\gamma$-profiles at the downwash are similar to their results.

The fact that the maximum $\gamma$ across the boundary layer in the early stages of transition does not occur near the wall, but at a distance away from the wall, might be explained by the shape of the turbulent spots in the early stages of transition. Cantwell et al. (1978) indicated that the shape of a turbulent spot generated near the wall had a maximum cross-sectional area away from the wall after it became fully developed. In the early stages of a turbulent spot evolution, there is a strong overhang in the shape of the turbulent spot. The same phenomenon was also observed in the present flow when simultaneous turbulent signals obtained by two hot wires placed near the wall were analyzed. It is inferred that such overhang and the influence of secondary instabilities results in the shape of intermittency profiles, as shown in Figures 6 and

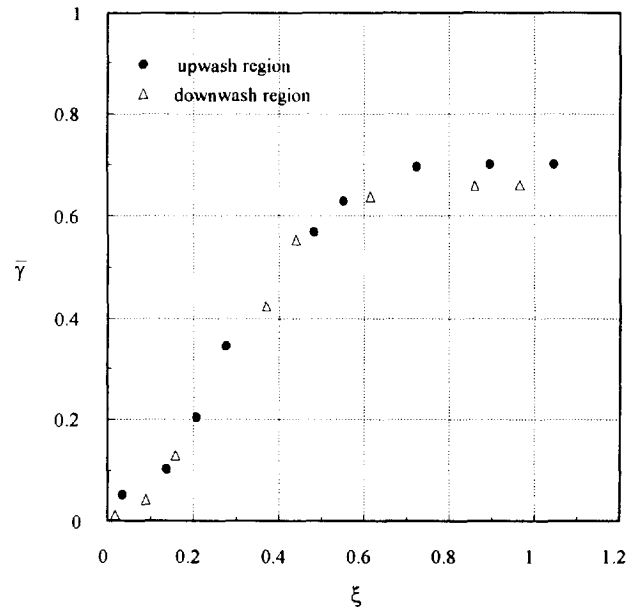


*Figure 8* Variations of mean boundary-layer intermittency value in the transition region

at various streamwise locations. The present findings, in which $\gamma$ is decreasing in the near wall regions of the boundary layer, is also consistent with those reported by Crane et al. (1987) and Walker and Solomon (1992) for concave surface boundary layers.

The delay of $\gamma$ toward zero in the outer region is possibly because of the entrainment of the free-stream flow into the boundary layer. From the intermittency profiles in Figures 6 and 7, it can also be seen that in the very late stages of transition ($\gamma > 0.95$), the intermittency factor is fairly constant in the near wall region and decreases gradually in the outer region. These results are in agreement with those of Kuan and Wang (1990), Sohn et al. (1991) and Dhawan and Narasimha (1958) for flat-plate boundary layers, and implies that the turbulent spots were fully developed.

It is also observed from Figures 6 and 7 that the intermittency factor $\gamma$ grows quite rapidly in the early stages of transition, both at the upwash and downwash, implying that the breakdown rate of Goertler vortices and the growth rate of the turbulent spots are large. The maximum $\gamma$ across the boundary layer reaches values of about 0.9 at $\xi = 0.55$ at the upwash, and about 0.85 at $\xi = 0.61$ at the downwash. In the later half range of transition, the growth of intermittency factor seems to be relatively slow.

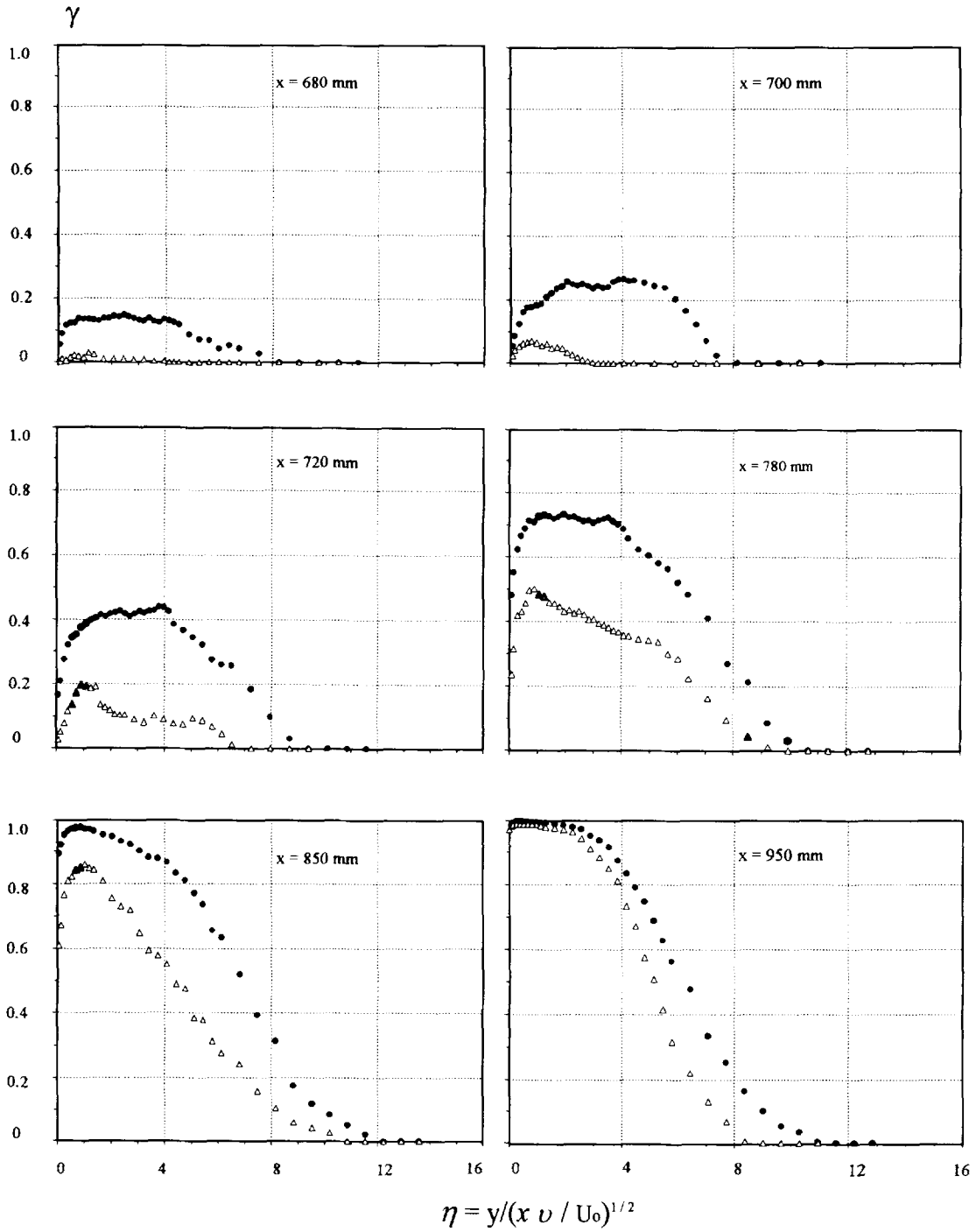


*Figure 9* Intermittency profile comparisons for the upwash (•) and downwash (△) regions at various streamwise positions

In addition to the above, comparisons between Figures 6 and 7 show that the intermittency profiles at the upwash seem to have larger integral areas across the boundary layers. To investigate the variations of such integral areas, a mean intermittency value $\bar{\gamma}$ across the boundary layer which is defined as follows:

$$\bar{\gamma} = \frac{1}{\delta}\int_0^{\delta} \gamma \, dy$$

was introduced, where $\delta$ is the measured boundary-layer thickness. The streamwise variations of $\bar{\gamma}$ in the upwash and downwash regions (Figure 8) show that, at both upwash and downwash, $\bar{\gamma}$ varies in similar way with $\xi$, regardless of the shapes of the $\gamma$ profiles (see Figures 6 and 7). It grows rapidly in the early stages of transition, and at $\xi = 0.5$, $\bar{\gamma}$ is nearly 0.6. It then decreases slowly and, at about $\xi = 0.7$, it asymptotically approaches a value of about 0.7 at the end range of transition.

To examine the effects of Goertler vortices on the intermittency profiles further, the profiles at some stream-wise locations at the upwash and downwash are compared (Figure 9). At $x = 680$ mm, it can be seen from the profiles that the transition first started at upwash; that is, when the upwash have already become transitional, the downwash can still be in laminar state. This is in agreement with the results reported by Crane et al. (1987) and Winoto and Low (1989). Figure 9 also shows that the large difference between the profiles at the upwash and downwash exists in the early stages of transition. This was also verified by inspecting the instantaneous velocity signals of the raw data.

## Conclusions

The streamwise mean and fluctuating velocities have been measured using hot-wire anemometry technique, in a laminar and transitional boundary-layer flow on a concave surface. From the measurements, the profiles of intermittency factor were obtained by using a new turbulent intermittency detector method.

The normal and spanwise distributions of velocity indicate that the initially Blasius boundary layer on the concave surface rapidly becomes 3-D as a system of counter-rotating streamwise vortices is established in accordance with the linearized stability analysis of Goertler. These vortices grow continuously downstream, producing regions of low- and high-speed fluid (or downwash and upwash regions) in the spanwise direction and resulting in the streamwise velocity profile $\tilde{u}(z)$ inflexional and a defect in $\tilde{u}(y)$ profiles from the Blasius value at the upwash region. After reaching a saturation state where transition starts, the vortices will cease to grow, and begin to attenuate with $x$.

The streamwise development of $u'_{rms}/U_0$ profiles at the upwash and downwash regions show a strong link with that of mean velocity. In the laminar boundary layer, the maximum value of $u'_{rms}/U_0$ across the boundary layer increases with $x$ both at the upwash and downwash. In the early transitional region, two peaks can be found in the upwash profiles, and the second peak may be a representation of existence of some secondary instabilities. As the flow becomes more turbulent, the second peak disappears gradually, and the maximum value of $u'_{rms}/U_0$ at both spanwise positions decreases and eventually reach the fully turbulent value. The comparisons between the $u'_{rms}/U_0$ profiles at the two regions indicate that their streamwise development processes are different. The variation of $u'_{rms}/U_0$ at the upwash region is more distinct.

The rapid neutralization of Goertler vortices in the transition region suggests the possible existence of secondary instability in the form of horseshoe-type structures or some other viscosity-induced spanwise vorticities generated by Helmholtz instability, which interact with the streamwise Goertler vortices caused by centrifugal effect during transitional flow.

The measured values of $G_\theta$ at the start of transition region are much higher in the upwash region (where $G_\theta = 10.04$) and much lower in the downwash region (where $G_\theta = 2.61$) than that based on Blasius value ($G_\theta = 6.93$). This suggests that when a transition Goertler number is used to determine the start of transition, the difference between the upwash and downwash regions should be taken into consideration. However, this may not be practical for design calculations.

Both at the upwash and downwash, the maximum value of intermittency factor $\gamma$ across the boundary layer occurs at a certain distance from the wall in the early stages of transition. At the downwash, the profiles have a peak value around $\eta = 1$, when $\gamma < 0.9$, while at the upwash, a fairly constant maximum value of the profiles exists midway of the boundary layer. The distribution of $\gamma(y)$, monotonically decreasing in the outer boundary layer and maintaining a nearly constant value in the near wall, is the characteristic of the late transition region.

The comparisons of the $\gamma$ profiles at the upwash and downwash regions again confirm that transition first starts at the upwash.

## References


Aihara, Y. 1979. Goertler vortices in the non-linear region. In *Recent Developments in Theoretical and Experimental Fluid Mechanics*, U. Muller, G. J. Roesher, and A. B. Schmidt (eds.), Springer, New York, 331–338

Aihara, Y. and Koyama, H. 1982. Nonlinear development and secondary instability of Goertler vortices. *IUTAM Symp. on Stability in the Mechanics of Continua*, Numbrecht, 345–354

Aihara, Y. and Sonoda, T. 1981. Effects of pressure gradients on the secondary instability of Goertler vortices. AIAA Paper 81-0197, AIAA 19th Aerospace Sciences Meeting, Reno, NV

Cantwell, B. J., Coles, D. and Dimotakis, P. E. 1978. Structure and entrainment in the plane of symmetry of a turbulent spot. *J. Fluid Mech.*, **89**, 641–672

Crane, R. I., Leoutsakos, G. and Sabzvari, J. 1987. Transition in pressure-surface boundary layers. *J. Turbomach.*, **109**, 296–302

Dhawan, S. and Narasimha, R. 1958. Some properties of boundary layer flow during the transition from laminar to turbulent motion. *J. Fluid Mech.*, **3**, 418–436

Floryan, J. M. 1991. On the Goertler instability of boundary layers. *Prog. Aerosp. Sci.*, **28**, 235–271

Floryan, J. M. and Saric, W. S. 1982. Stability of Goertler vortices in boundary layers. *AIAA J.*, **20**, 316–324

Goertler, H. 1940. *Nachr. Acad. Wiss. Gottingen. Math. Phys. K*1, **2**, translated as "On the three-dimensional instability of laminar boundary layer on concave walls." NACA Tech. Memo. 1375, 1954

Ito, A. 1985. Breakdown structure of longitudinal vortices along a concave wall. *J. Japan Soc. Aerosp. Sci.*, **33**, 166–173

Klebanoff, P. S., Tidstrom, K. D. and Sargent, L. H. 1962. The three- dimensional nature of boundary layer instability. *J. Fluid Mech.*, **12**, 1–34

Kuan, C. L. and Wang, T. 1990. Investigation of the intermittent behavior of transitional boundary layer using a conditional averaging technique. *Exp. Therm. Fluid Sci.*, **3**, 157–173

Liepmann, H. W. 1945. Investigation of boundary layer transition on concave walls. NACA Wartime Rep., Adv. Conf. Rep. 4J28

McCormack, P. D., Welker, H. and Kelleher, M. 1970. Taylor–Goertler vortices and their effect on heat transfer. *ASME J. Heat Trans.*, **92**, 101–112

Saric, W. S. 1994. Goertler vortices. *Annu. Rev. Fluid Mech.*, **26**, 379–409

Smith, A. M. O. 1955. On the growth of Taylor–Goertler vortices along highly concave walls. *Quart. Appl. Math.*, **13**, 233–262

Smith, S. T. and Haj-Hariri, H. 1993. Goertler vortices and heat transfer: A weakly nonlinear analysis, *Phys. Fluid, A*, **5**, 2815–2825

Sohn, K. H., Reshotko, E. and Zaman, K. B. M. Q. 1991. Experimental study of boundary layer transition on a heated flat plate. FED-Vol. **14**, *Boundary Layer Stability and Transition to Turbulence*, American Society of Mechanical Engineering, New York, 163–172

Swearingen, J. D. and Blackwelder, R. F. 1987. The growth and breakdown of streamwise vortices in the presence of a wall. *J. Fluid Mech.*, **182**, 255–290

Tani, I. and Aihara, Y. 1969. Goertler vortices and boundary layer transition. *Z. Angew. Math. Phys.*, **20**, 609–618

Walker, G. J. and Solomon, W. J. 1992. Turbulent intermittency measurement on an axial compressor blade. *Proc. 11th Austr. Fluid Mech. Conf.*, Hobart, Tasmania, Australia, 1277–1280

Winoto, S. H. and Crane, R. I. 1980. Vortex structure in laminar boundary layers on a concave wall. *Int. J. Heat Fluid Flow*, **2**, 221–231

Winoto, S. H. and Low, H. T. 1989. Transition of boundary layer flows in the presence of Goertler vortices. *Experiments in Fluids*, **8**, 41–47

Zhang, D. H., Chew, Y. T. and Winoto, S. H. 1994. A proposed intermittency measurement method for transitional boundary layer flows. *Experiments in Fluids* (in press).